⌘ *Author's Choice*

# Increased Monomerization of Mutant HSPB1 Leads to Protein Hyperactivity in Charcot-Marie-Tooth Neuropathy*⬧

**Leonardo Almeida-Souza**[‡§1], **Sofie Goethals**[‡§], **Vicky de Winter**[‡§], **Ines Dierick**[‡§2], **Rodrigo Gallardo**[¶], **Joost Van Durme**[¶3], **Joy Irobi**[‡§3], **Jan Gettemans**[∥], **Frederic Rousseau**[¶], **Joost Schymkowitz**[¶], **Vincent Timmerman**[‡§4], **and Sophie Janssens**[‡§3,5]

*From the ‡Peripheral Neuropathy Group, VIB Department of Molecular Genetics and University of Antwerp, 2610 Antwerp, Belgium, the §Neurogenetics Laboratory, Institute Born-Bunge, 2610 Antwerp, Belgium, the ¶VIB Switch Laboratory, Vrije Universiteit Brussel, 1050 Brussels, Belgium, and the ∥VIB Department of Medical Protein Research and Department of Biochemistry, Faculty of Medicine and Health Sciences, Ghent University, 9000 Ghent, Belgium*

**Small heat shock proteins are molecular chaperones capable of maintaining denatured proteins in a folding-competent state. We have previously shown that missense mutations in the small heat shock protein HSPB1 (HSP27) cause distal hereditary motor neuropathy and axonal Charcot-Marie-Tooth disease. Here we investigated the biochemical consequences of HSPB1 mutations that are known to cause peripheral neuropathy. In contrast to other chaperonopathies, our results revealed that particular HSPB1 mutations presented higher chaperone activity compared with wild type. Hyperactivation of HSPB1 was accompanied by a change from its wild-type dimeric state to a monomer without dissociation of the 24-meric state. Purification of protein complexes from wild-type and HSPB1 mutants showed that the hyperactive isoforms also presented enhanced binding to client proteins. Furthermore, we show that the wild-type HSPB1 protein undergoes monomerization during heat-shock activation, strongly suggesting that the monomer is the active form of the HSPB1 protein.**

Inherited peripheral neuropathies comprise a very complex and genetically diverse group of disorders affecting the peripheral nervous system. Charcot-Marie-Tooth (CMT)[6] disease is the most common type and is clinically characterized by a symmetric weakness and wasting of distal muscles in lower limbs, feet, and hands. Mutations in more than 40 genes have been linked to CMT neuropathy and related disorders (1). Dominant missense mutations in the small heat shock protein 27 (HSP27 or HSPB1) were linked to CMT type 2F and distal hereditary motor neuropathy (2, 3).

Small heat shock proteins (sHSPs) are stress-induced chaperones with a ubiquitous expression pattern that are characterized by the presence of a conserved α-crystallin domain. Unlike the heat shock proteins with an ATPase domain (*e.g.* HSP70), sHSPs do not have the intrinsic capacity to refold denatured proteins. However, they are able to bind unfolded substrates and keep them in a folding-competent state. These sHSP-unfolded protein complexes act as repositories that are later cleared out by the ATP-dependent heat shock proteins (4).

Like all other members of the sHSP family, HSPB1 exists in a dynamic equilibrium between oligomeric and dimeric states. Although HSPB1 oligomers ranging from 12- to 30-mers have been described, the 24-meric state arranged in dimers is the most common form (5, 6). The exact role of each of these states in the function of sHSPs is still controversial. Some studies support the idea that the dissociation of the oligomer is required for substrate recognition (7), whereas others have shown that the oligomeric state is the chaperone active form that protects cells from stress (8, 9).

Besides its canonical folding properties, HSPB1 is involved in several cellular processes, such as apoptosis (10, 11), cytoskeleton dynamics (12), and translational elongation (13). Therefore, pinpointing the underlying mechanism for the neuron-specific phenotype of CMT causing HSPB1 mutations represents a big challenge (14, 15).

In this study, we investigated the influence of the CMT causing HSPB1 mutations identified by us in 2004 (2) on the basic biochemical properties of this protein using neuronal cell lines stably expressing either wild-type or mutant HSPB1 variants. Surprisingly, three missense mutations presented higher *in vivo* chaperone activity when compared with the wild-type protein. The enhanced activity of these mutations was accompanied by an increased fraction of the protein residing in a monomeric state. Consistently, analysis of the predicted protein structure of HSPB1 suggested a mechanism for the monomeric tendency of hyperactive mutants. Furthermore, we were able to show

that heat shock-induced activation of the wild-type HSPB1 is also accompanied by a similar increase in the fraction of the protein residing in the monomeric state, at the expense of the dimer fraction, indicating that the ratio between monomeric and dimeric HSPB1 is a key determinant for the activity of the protein.

## EXPERIMENTAL PROCEDURES

*Identification of the Non-pathogenic Variation S156Y*—Using direct DNA sequencing, we identified an HSPB1 variation, c.467C>A, in one CMT2 affected patient (CMT-442.01) from a Croatian family (supplemental Fig. S1). The mutation was found to be non-pathogenic because this variation was not present in the affected sister (CMT-442.02). Mutation analysis was performed by sequencing of amplification products containing exons and intron-exon boundaries of all HSPB1 exons. Sequencing reactions were performed using the Big Dye Terminator kit (Applied Biosystems) and run on an ABI3730xl sequencer (Applied Biosystems). Sequencing data were analyzed using NovoSNP software (16).

*Cell Culture Material and Conditions*—All cell culture media and supplements were acquired from Invitrogen. The human neuroblastoma cell line SH-SY5Y was acquired from ATCC, whereas HEK293 Flp-in host cells were purchased from Invitrogen. When not stated differently, SH-SY5Y cells were cultivated at 37 °C and 5% $CO_2$ in minimum essential medium supplemented with 10% fetal calf serum, non-essential amino acids, glutamine, and penicillin/streptomycin. HEK293 Flp-in cells were cultivated at 37 °C and 5% $CO_2$ in Dulbecco's modified Eagle's medium supplemented with 10% fetal calf serum, glutamine, and penicillin/streptomycin.

*SH-SY5Y Stable Cell Lines*—To generate stable SH-SY5Y cell lines, we made constructs encoding different HSPB1 mutations or EGFP using the Gateway recombination system (Invitrogen). Using primers containing the attB recombination sites, ORFs from HSPB1 wild-type, R127W, S135F, R136W, T151I, and P182L were amplified from constructs described elsewhere (2). The non-pathogenic HSPB1 variation S156Y was generated by site-directed mutagenesis. The EGFP cassette was amplified from the vector pEGFP-N1 (Clontech). The PCR products containing the ORFs flanked by the attB recombination sites were then recombined into a pDONR221 vector, and the sequence was validated. The validated pDONRs-HSPB1 constructs were then transferred by recombination to the pLENTI6/V5-Dest (Invitrogen) generating constructs with the ORFs C-terminally fused to a V5 tag. Stable cell lines were produced by lentiviral transduction of the neuronal cell line SH-SY5Y, according to the method described previously (17). The construct for stable expression of the luciferase gene was generated by amplifying the luciferase gene ORF from the vector pNF-conluc (gift from A. Israel (Institut Pasteur, Paris)) and recombining it into the vector pLENTI6/V5-Dest (Invitrogen). Double stable cell lines expressing both luciferase and the HSPB1 forms were generated by lentiviral transduction of the HSPB1-expressing stable cell lines with the luciferase construct. Stable cells lines presented similar expression levels and equal growth rate (data not shown).

*HEK293 Flp-in Stable Cell Lines*—To generate stable HEK293 Flp-in cell lines, we made constructs carrying a double tag (FLAG-TEV cleavage site-Protein A) (18) C-terminally fused to HSPB1 isoforms or EGFP. To this end, the double tag cassette from the vector pMET-TYK7-TAP2 (gift from Jan Tavernier (Ghent University)) and the single recombination Gateway cloning cassette were transferred to the Flp-in vector pCDNA5/FRT. The resulting vector was called pCDNA5/FRT/GW/TAP2. ORFs from different HSPB1 isoforms and the EGFP were cloned into the pCDNA5/FRT/GW/TAP2 vector using Gateway recombination following the manufacturer's instructions (Invitrogen). Stable cell lines were generated by using the Flp-in host cell line HEK293 following manufacturer instructions (Invitrogen).

*Thermotolerance Assay*—SH-SY5Y cells stably expressing the HSPB1 isoforms or the EGFP control were seeded at the same confluence ($1 \times 10^4$ cells/well) in triplicates in four different 24-well plates. On the next day, three plates were heat-shocked in a water bath at 45 °C for 30, 60, or 90 min. After heat shock, cells were put back in the incubator at 37 °C for recovery. The fourth plate was kept at 37 °C as a non-heat shock control. The survival of cells was evaluated 48 h after heat shock using the CyQuant cell proliferation assay (Invitrogen) following the manufacturer's instructions. This assay measures the fluorescence emitted by a DNA binding dye that is directly correlated to cell number. Cell survival was expressed as the ratio of the fluorescent signal between the heat-shocked cells and the non-heat-shocked cells for each time point. The experiment was done twice, and results represent the pooled results from the two experiments. Statistical significance was determined using a two-tailed Student's $t$ test and false discovery rate (FDR) (19).

*In Vivo Chaperone Activity*—The *in vivo* chaperone activity assay was adapted from Nollen *et al.* (20). Double stable SH-SY5Y cell lines expressing luciferase and the HSPB1 isoforms or EGFP were seeded in triplicates, at the same confluence ($1 \times 10^4$ cells/well) in three different 24-well plates. On the next day, medium from the three plates was replaced by 500 $\mu$l of minimal Eagle's medium supplemented with 20 mM MOPS and 40 $\mu$g/ml cycloheximide. Cells were put back for 30 min in the 37 °C incubator to ensure complete inhibition of translation by cycloheximide. Subsequently, two plates were heat-shocked for 30 min at 44 °C while one was kept at the 37 °C incubator as a non-heat-shocked control. After the heat shock, one of the plates was allowed to recover at 37 °C for 180 min while from the other plates medium was removed immediately, and cells were frozen at −80 °C. After the 180-min recovery time, medium was removed from the third plate, and cells were frozen at −80 °C. Luciferase activity was measured using the dual luciferase reporter assay system (Promega) following the manufacturer's instructions. The luciferase activity was expressed as a ratio of the luminescence between the heat-shocked conditions and the non-heat-shocked control. Statistical significance was determined using a two-tailed Student's $t$ test and FDR (19).

*Size Exclusion Chromatography*—For size exclusion chromatography (SEC) experiments, stable SH-SY5Y cells were grown in 150-cm$^2$ dishes, harvested with a cell scraper, and washed two times with phosphate-buffered saline. The pellets were resuspended in 500 $\mu$l of hypotonic buffer (20 mM HEPES, 10

mM KCl, 1 mM MgCl$_2$, 1 mM EDTA, 1 mM EGTA, 1 mM dithiothreitol (DTT), pH 7.5). Cells were lysed by three gentle sonication cycles (30% amplitude for 10 s, alternating a 1-s pulse and 1-s rest). Lysates were cleared by centrifugation at 20,000 × $g$ for 15 min. The lysates were then adjusted to the same protein concentration (3 mg/ml), and the salt concentration was increased to 150 mM NaCl. SEC was performed in a fast protein liquid chromatography AKTA system by injecting 500 $\mu$l of the cell lysates into a Superdex 200 HR column (GE Healthcare) with constant flow (0.5 ml/min) of the hypotonic buffer adjusted to 150 mM NaCl. Fractions of 1 ml were collected and further analyzed for the presence of HSPB1 by Western blot. The $M_r$ calibration of the column was done by running a gel filtration $M_r$ standard (Bio-Rad).

*Tandem Affinity Purification*—HEK293 stable cell lines were grown in 150-cm$^2$ dishes, harvested with a cell scraper, and washed two times with phosphate-buffered saline. Cell pellets were lysed in 500 $\mu$l of tandem affinity purification lysis buffer (50 mM Tris-HCl (pH 8.0), 10% glycerol, 1% Nonidet P-40, 150 mM NaCl, 5 mM NaF, 5 $\mu$M ZnCl$_2$, 1 mM Na$_3$VO$_4$, 10 mM EGTA, and protease inhibitor mixture (Roche Applied Science)). Cytosolic lysates (3 mg) from each stable cell line were incubated with 25 $\mu$l of IgG-Sepharose beads (GE Healthcare) for 4 h at 4 °C with constant agitation. Beads were washed three times with washing buffer (20 mM Tris-HCl, pH 7.5, 5% glycerol, 0.1% Nonidet P-40, and 150 mM NaCl) and three additional times with TEV protease cleavage buffer (10 mM Tris-HCl, pH 8, 150 mM NaCl, 0.1% Nonidet P-40, and 0.5 mM EDTA). The washed IgG-Sepharose beads were then incubated overnight at 4 °C and constant agitation with 10 units of AcTEV protease (Invitrogen) in 200 $\mu$l of TEV protease cleavage buffer. After TEV cleavage, the supernatants containing the eluted complexes were incubated with 25 $\mu$l of anti-FLAG beads (Sigma) for 4 h at 4 °C with constant agitation. After incubation, beads were washed gently three times with washing buffer. Final elution was done by incubation of the FLAG beads for 30 min at 4 °C with 250 ng/$\mu$l of the 3× FLAG peptide. Final eluates were run on 10% NuPAGE gels (Invitrogen) and silver-stained for protein visualization.

*Detection of HSPB1 Dimers and Monomers by Western Blot*—Cells were lysed in Nonidet P-40 lysis buffer (50 mM Tris-HCl (pH 8.0), 10% glycerol, 1% Nonidet P-40, 150 mM NaCl, 5 mM NaF, 5 $\mu$M ZnCl$_2$, 1 mM Na$_3$VO$_4$, 10 mM EGTA, and Complete protease inhibitor mixture (Roche Applied Science)) for 10 min on ice and cleared by centrifugation. For detection of dimers, cell extracts were boiled for 5 min in non-reducing SDS loading buffer (5× solution: 250 mM Tris-HCl, pH 6.8, 10% SDS, 30% glycerol, 0.02% bromphenol blue). To dissociate the dimers, DTT was added to 100 mM final concentration.

*HSPB1 Heat Shock Activation Assay*—Stable cells expressing wild-type HSPB1 were seeded in four 10-cm$^2$ dishes at the same confluence (3 × 10$^5$ cells/dish). The next day, three dishes were heat-shocked at 44 °C for 30 min while one dish was kept in the 37 °C incubator as a non-heat-shocked control. The three heat-shocked dishes were allowed to recover from heat shock for 0, 30, or 60 min. After the recovery period medium was removed, cells were washed with phosphate-buffered saline and lysed directly on a plate with Nonidet P-40 lysis buffer. Cell extracts

for each time point were run on gel in both reducing and non-reducing conditions. For the HSPB1 heat shock activation assay in non-phosphorylated conditions, we followed the same protocol as described above; however, cells were pretreated for 2 h with the p38 inhibitor SB203580 (20 $\mu$M; Enzo Life Sciences) or vehicle control (DMSO).

*HSPB1 Structural Modeling*—The model of HSPB1 was constructed using the atomic coordinates of the human $\alpha$B-crystallin $\alpha$-crystallin domain structure with Protein Data Bank code 2WJ7 (21). It is currently the closest homolog to the human HSPB1 in the Protein Data Bank. The percentage of sequence identity between template and target monomers is 54% (71% sequence similarity), allowing an unambiguous sequence alignment. FoldX (22) was used to construct the model. During the homology modeling process, the side chains of the conserved residues were kept fixed, whereas the substitutions were modeled using a backbone-dependent rotamer library and the FoldX force field to calculate the resulting free energy. All mutants were modeled in the monomeric as well as in the dimeric forms of HSPB1. Structures were analyzed using Deepview software (23), and molecular graphics were rendered using PovRay.

*Western Blot Reagents and Band Quantification*—Western blot reagents were acquired from GE Healthcare. Mouse monoclonal anti-HSPB1 antibody was purchased from Stressgen, mouse monoclonal anti-V5 was acquired from Invitrogen, and mouse monoclonal anti-tubulin was obtained from Abnova (anti-$\alpha$-tubulin). Band intensity on Western blots was determined by quantifying gray pixel values using the gel analyzer module of ImageJ software (24).

## RESULTS

*Stable Cell Lines Expressing HSPB1 Mutations R127W and S135F Display Increased Thermotolerance*—Cells overexpressing HSPB1 are known to have higher thermotolerance than cells expressing HSPB1 at endogenous levels (9). We therefore tested whether CMT-causing HSPB1 mutations influence this property. To this end, we generated neuronal cell lines stably expressing wild-type HSPB1 as well as several CMT-causing mutants (R127W, S135F, R136W, T151I, and P182L), one non-pathogenic variation (S156Y), and EGFP as a negative control. The cells were seeded in different plates and heat-shocked for 30, 60, or 90 min at 45 °C or left untreated. Survival of the cells was evaluated using a fluorescence-based cell counting assay and expressed as the ratio of the fluorescent signal between heat-shocked and non-heat-shocked cells. As expected, cells expressing wild-type HSPB1 were significantly more thermotolerant than cells expressing the EGFP-negative control (Fig. 1*A*). No difference in thermotolerance was detected between cells expressing wild-type HSPB1 and the mutations R136W, T151I, or the non-pathogenic variation S156Y. Cells expressing the P182L mutation lost their thermotolerance capacity and showed a survival rate similar to the EGFP-negative control-expressing cells. In contrast, two mutations, R127W and S135F, rendered cells more thermotolerant than cells expressing wild-type HSPB1 protein. This difference was especially pronounced for the cells heat-shocked for 60 or 90 min.

**A**



**B**



**C**
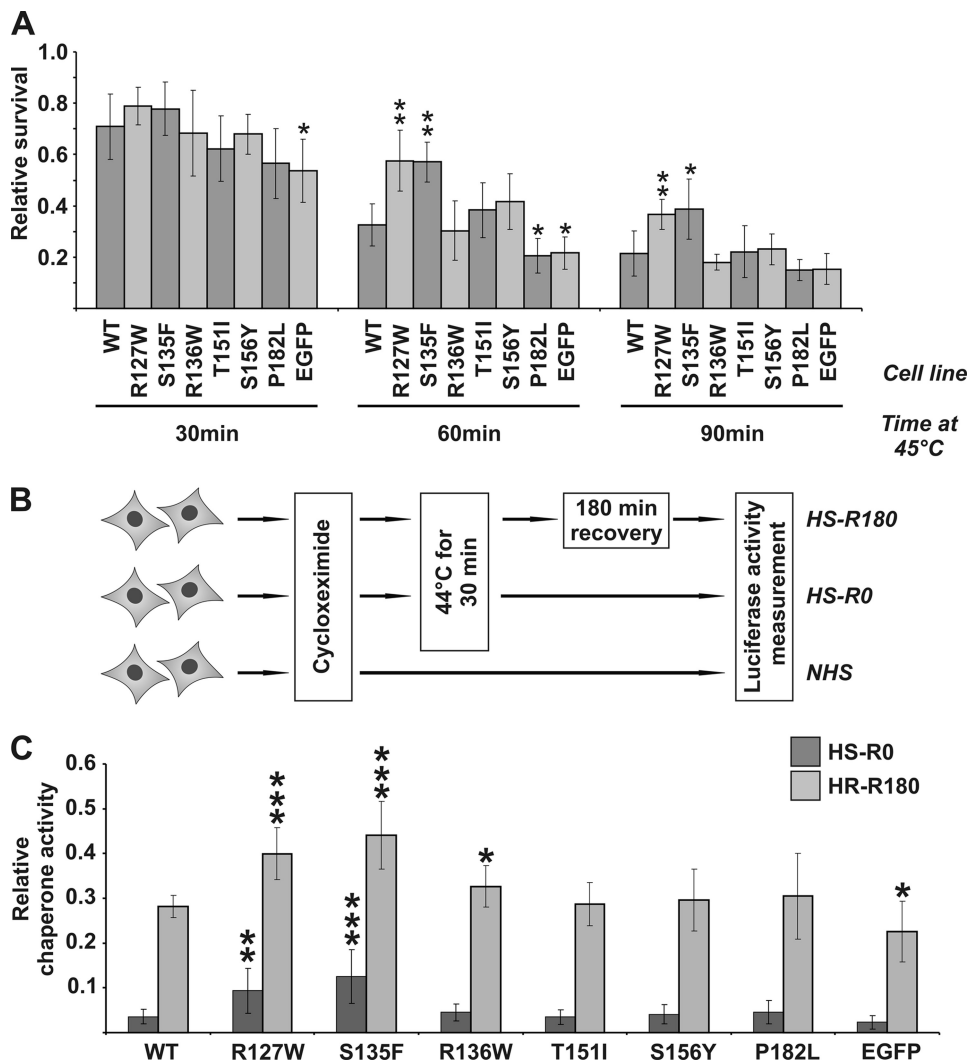


FIGURE 1. **Thermotolerance and chaperone activity of cell lines stably expressing CMT-causing HSPB1 mutations.** *A*, to measure the HSPB1-mediated thermotolerance, cells stably expressing different HSPB1 iso-forms were heat-shocked for 30, 60, and 90 min or left untreated. The cell number was determined 48 h after treatment using a fluorescence-based method. Cell survival was expressed by dividing the fluorescence signal from each time point by the respective non-heat-shocked control. Cells expressing HSPB1 mutations R127W and S135F presented higher thermotolerance than the cells expressing the wild-type protein, whereas cells expressing the P182L mutation were more sensitive. Results are mean values with ±S.D. *error bars* from two independent experiments with three repetitions each. *B*, experimental setup for the *in vivo* chaperone experiments. Cycloheximide was added to the cells before treatment to avoid translation of additional endogenous chaperones during the heat shock. Chaperone activity was calculated by dividing the luciferase activity from each condition to the respective non-heat-shocked control. *C*, *in vivo* chaperone activity for cells stably expressing different HSPB1 isoforms. Cells expressing HSPB1 mutations R127W, S135F, and R136W showed higher chaperone activity than cells expressing the wild-type protein. Results are mean values with ±S.D. *error bars* from three independent experiments with three repetitions each. Statistical differences to the wild-type HSPB1 stable cell line were tested using Student's *t* test and corrected for multiple comparisons using the FDR test (supplemental Fig. S2). *, $p < 0.05$; **, $p < 0.01$; ***, $p < 0.001$; *HS-R0*, heat shock and no recovery; *HS-R180*, heat shock and 180-min recovery; *NHS*, non-heat-shocked control. *WT*, wild type.

*HSPB1 Mutations R127W, S135F, and R136W Show Higher in Vivo Chaperone Activity*—The capacity of sHSP to protect proteins from complete denaturation is proposed to be responsible for conferring thermotolerance to cells (9). Therefore, to test whether the differences in thermotolerance are accompanied by differences in chaperone activity for these mutant proteins, we used an *in vivo* assay that uses the refolding of lucifer-ase as readout for chaperone activity within cells (20). SH-SY5Y stable cells expressing the luciferase gene and the different HSPB1 isoforms or EGFP were treated as described in the

experimental setup outlined in the legend to Fig. 1*B*. The chaperone activity was calculated by dividing the luciferase luminescence from the heat-shocked cells by the one from the non-heat-shocked cells.

As shown in Fig. 1*C*, expression of wild-type HSPB1 conferred additional chaperone activity to cells when compared with cells harboring the EGFP construct (*t* test $p = 0.04$ and FDR $p = 0.084$ (see supplemental Fig. S2)). Cells expressing mutations T151I, P182L, and the non-pathogenic variation S156Y showed no significant difference in chaperone activity compared with cells expressing wild-type HSPB1 at both time points tested (HS-R0 or HS-R180). Cells expressing the R136W mutation showed a slightly higher chaperone activity than the wild-type protein (*t* test $p = 0.02$ and FDR $p = 0.065$ (see supplemental Fig. S2)). On the other hand, cells expressing mutations R127W and S135F showed a significantly higher ($p < 0.001$) chaper-one activity than the wild-type expressing cells. Interestingly, the chaperone activity for the mutants R127W and S135F was also higher at the "HS-R0" time point (*i.e.* no recovery after heat shock), suggesting that these proteins are either constitutively active or activated faster. These results contrast to what was previously reported for other chaperonopathies, where pathogenic mutations are associated with loss in chaperone activity (25–27).

*HSPB1 Mutations R127W and S135F Lead to an Increased Fraction of the Protein Adopting a Monomeric Conformation*—Under stress conditions, sHSPs become activated and change their equilibrium between oligomeric and dimeric states (4). To test whether the higher chaperone activity of the HSPB1 mutations R127W, S135F, and R136W is accompanied by changes in their oligomeric state, we performed SEC using extracts from SH-SY5Y cells expressing mutant and the wild-type protein. The elution profile of HSPB1 for each stable cell line was determined by Western blotting of the different SEC fractions (Fig. 2*A*). The wild-type protein eluted predominantly in two regions corresponding to the previously described oligomeric 24-mer state (~700 kDa) and the dimeric state (~60 kDa) (5, 6). The mutants
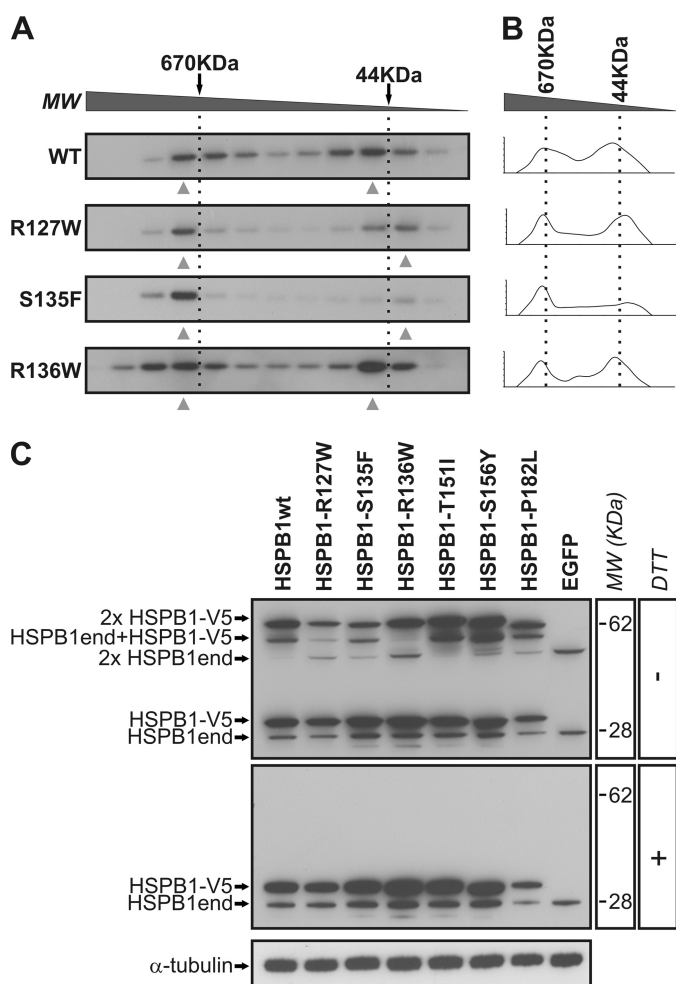
FIGURE 2. **Oligomeric state of CMT causing HSPB1 mutations.** *A*, SEC profile from the wild type and R127W, S135F, and R136W mutants. Fractions were run on gel and subjected to Western blot using anti-V5 antibody. *Black arrows* and *dotted lines*, $M_r$ as determined by a calibration run using proteins of known molecular size. The *gray arrowheads* indicate the strongest bands as determined by densitometry using ImageJ software. *B*, graphs showing the amount of the HSPB1 protein along the SEC fractionation and the elution peak shift for the R127W and S135F mutants. Signals for each fraction were normalized for the highest signal intensity and plotted as a *smoothed curve*. *C*, Western blot showing HSPB1 dimers. Western blots performed with nonreduced samples (*top*) permit the visualization of the three possible HSPB1 dimers: the dimer between two exogenous V5-tagged HSPB1 molecules (*2× HSPB1-V5*), the dimer between two endogenous HSPB1 molecules (*2× HSPB1end*), and the dimer between exogenous V5-tagged HSPB1 and endogenous HSPB1 (*HSPB1end + HSPB1-V5*). Note the higher monomerization for the R127W and S135F mutations. The R136W mutation presented a lower dimerization only with the endogenous protein. *WT*, wild type.

R127W, S135F, and R136W equally displayed an elution profile with two major peaks, with no major observable differences in the peak corresponding to the larger apparent molecular weight when compared with the wild type. However, as can be seen from Fig. 2, *A* and *B*, the fractions of the R127W and S135F mutants eluting at low apparent molecular weight shifted to higher elution volumes when compared with the wild-type protein, indicative of a decrease in the apparent molecular weight of the fraction. According to the $M_r$ standard, the $M_r$ of the later eluting fraction of both mutants corresponds to ~30 kDa, fitting the size of one HSPB1 molecule and suggesting that the mutant proteins are present as monomers rather than dimers. In contrast, the R136W mutation showed an elution profile

similar to that of the wild-type HSPB1 protein. The SEC was also performed for the other HSPB1 mutants, and no difference in the apparent molecular weight of the two main peaks in the elution profile was detected (supplemental Fig. S3).

Using site-directed spin labeling, Mchaourab *et al.* (28) and Berengian *et al.* (29) suggested the presence of disulfide bridges in the HSPB1 dimer interface. We also know by experience that the HSPB1 dimer is resistant to SDS treatment. For this reason, HSPB1 dimers can be visualized by Western blot by running gels with non-reduced (without DTT) samples. The lack of DTT in the samples generates three extra higher bands in the Western blot (around 60 kDa) corresponding to the three possible HSPB1 dimers. Given the fact that we introduced exogenous HSPB1 as a fusion protein, its molecular mass differs from the endogenous protein by 5 kDa. Hence, the highest molecular weight band corresponds to exogenous homodimer, the lower molecular weight band to the endogenous homodimer, and the intermediate band to the heterodimer of HSPB1. As shown in Fig. 2*C*, the R127W and S135F mutants showed a strong reduction in the two dimeric forms containing the mutant protein (2× HSPB1-V5 and HSPB1end + HSPB1-V5) as compared with wild-type HSPB1, whereas for the other mutants no striking differences were seen. Interestingly, R136W showed loss of dimerization only with the endogenous HSPB1 protein, whereas the interaction between both exogenous forms was intact (Fig. 2*C*). HSPB1 P182L was consistently detected at a lower level, due to the insolubility of the protein. The same results were obtained using a different cell line (HEK293 cells) stably expressing HSPB1 fused to a different tag (supplemental Fig. S4). Interestingly, the deficiency in dimerization shown by the mutants R127W, S135F, and R136W was compensated by an increase in the amount of fully endogenous dimers (Fig. 2*C*, band 2× *HSPB1end*).

*Structural Prediction of the HSPB1 Protein Suggests a Mechanism for the Monomerization of Hyperactive Mutant*—To try to understand how these mutations cause the destabilization of the HSPB1 dimer, we looked at the recently published crystal structure for the mammalian small heat shock protein αB-crystallin (21). The high conservation (71%) between the α-crystallin domain of αB-crystallin and HSPB1 permits the building of a predicted model of HSPB1 and the structural analysis of the effect of the CMT-causing mutations (Fig. 3). In contrast to the sHSPs previously published (30–33), where the dimer interface is composed of a β-sheet and a loop, the interface region between two subunits of αB-crystallin is an extended β-sheet formed by β-strands 6 and 7. The Ser-135 residue is located in the dimer interface and is predicted to form a pair of hydrogen bonds with the Thr-139 residue from the other subunit (Fig. 3*A*). The S135F mutation results in the projection of the aromatic R-group from phenylalanine toward the other subunit, possibly avoiding the formation of the hydrogen bonds and destabilizing the dimer (Fig. 3*C*). The Arg-127 residue is localized in the region preceding the dimerization β-strand. The R-group from this arginine is predicted to form an important hydrogen bond with the His-103 residue stabilizing part of the β6 and part of the β7 strands (Fig. 3*A*). The R127W mutation does not allow the formation of this hydrogen bond (Fig. 3*B*), possibly destabilizing a part of the β-strand from the interface
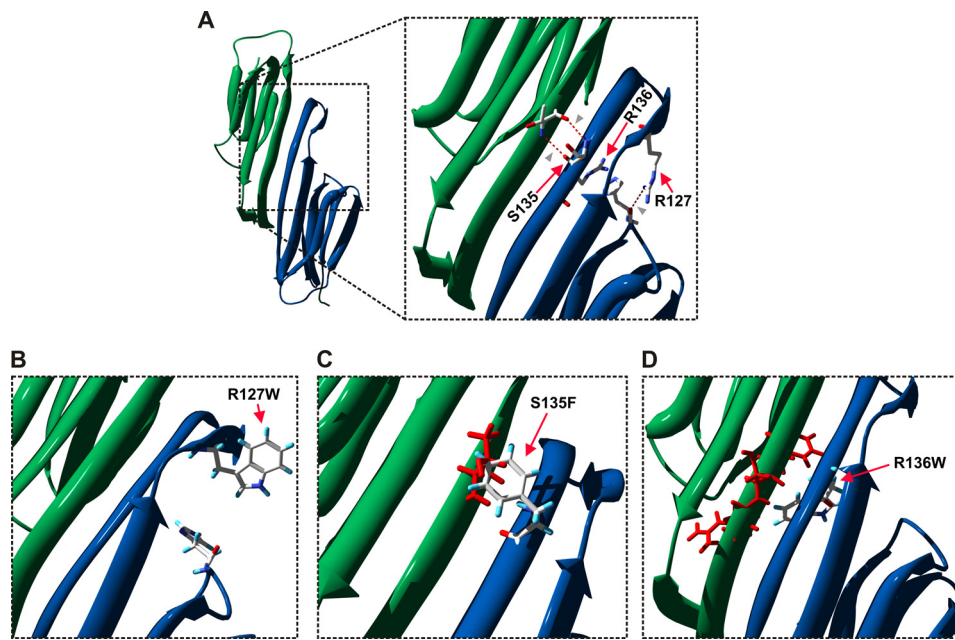
FIGURE 3. **Predicted structure of the HSPB1 α-crystallin domain dimer.** HSPB1 dimer structure was predicted based on the crystal structure of the αB-crystallin α-crystallin domain (21). Each dimer subunit is represented in a different *color* (*blue* and *green*). *A*, predicted HSPB1 dimer structure with *enlargement* showing the wild-type position of the residues Arg-127, Ser-135, and Arg-136 (*R127*, *S135*, and *R136*), indicated by *red arrows*. The *gray arrowheads* show hydrogen bonds. *B*, the mutation R127W does not allow the formation of a hydrogen bond necessary for the stability of the β-sheet present in the dimer interface. *C*, the mutation S135F results in the projection of the phenylalanine aromatic R-group (shown in *white*) toward the Thr-139 residue from the opposite dimer subunit (shown in *red*), possibly avoiding the formation of the hydrogen bonds and destabilizing the dimer. *D*, in contrast, the mutation R136W does not seem to cause any obvious change in the dimer interface, possibly explaining the milder effects found for this mutation (residues Arg-136, Cys-137, and Phe-138 from the opposite dimer subunit are shown in *red*).
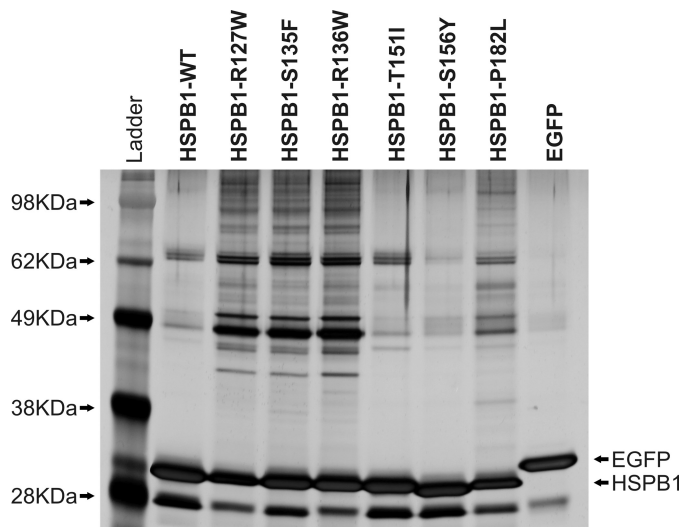


FIGURE 4. **Tandem affinity purification of protein complexes from cell lines stably expressing wild-type and CMT-causing HSPB1 mutations.** Tandem affinity purifications were performed using cell extracts from HEK293 cells stably expressing CMT-causing HSPB1 mutations C-terminally fused to a double affinity tag (FLAG-TEV-Protein A). Eluates were run on a 10% NuPage gel and silver-stained for protein visualization. Note the clear general enhanced binding of the three hyperactive mutations R127W, S135F, and R136W. *WT*, wild type.

and explaining the dimerization deficit of this mutant. The residue Arg-136, besides also being present in the dimerization β-strand, does not form any bond with other residues; nor does it project its R-group toward the dimer interface (Fig. 3*A*). The R136W mutation does not seem to cause any obvious change in the dimer interface, possibly explaining why this mutation has only a little effect on its chaperone activity and dimerization (Fig. 3*D*). Additionally, the predicted structure also showed that the cysteines from both subunits are facing each other (data not shown), allowing the formation of the disulfide bridge that keeps the HSPB1 dimer intact during the electrophoresis with non-reduced samples.

*Mutations R127W, S135F, and R136W Present Enhanced Binding to HSPB1 Client Proteins*—Small heat shock proteins exert their protective chaperone function by binding to exposed hydrophobic surfaces in damaged proteins and avoiding their irreversible damage. The proteins bound by heat shock proteins are referred to as client proteins. We investigated whether the hyperactivity of the HSPB1 mutants has an effect on their binding to client proteins. Protein complexes were purified by tandem affinity purification using HEK293 cells stably expressing wild type and the different HSPB1 isoforms or EGFP and visualized in silver-stained gels. The R127W, S135F, and R136W mutants showed a clear enhanced binding to their client proteins when compared with the wild-type HSPB1, the non-pathogenic variation S156Y, and the T151I mutation (Fig. 4). The purification from the P182L mutation also presented more client proteins but to a much lower extent than the R127W, S135F, and R136W mutations. These results show that the enhanced activity of these mutations is disturbing the normal binding of HSPB1 to its client proteins.

*Heat Shock Activation of Wild-type HSPB1 Is Also Accompanied by Monomerization and Is Phosphorylation-independent*—Our results demonstrate that some HSPB1 mutations present higher chaperone activity and concomitant increase of the monomeric fraction of the protein. To determine whether these two phenomena are related, we tested if the activation of wild-type HSPB1 is also accompanied by monomer formation. Therefore, SH-SY5Y cells expressing wild-type HSPB1 were heat-shocked at 44 °C for 30 min and allowed to recover for different periods of time. HSPB1 dimers and monomers for each time point were then visualized by Western blot with reduced and non-reduced samples. Fig. 5*A* shows that in basal conditions, wild-type HSPB1 is present predominantly in a dimeric form and that heat shock induces a transient increase of the monomeric fraction of wild-type HSPB1. The quantification of the ratio between monomers and dimers shows that the heat-induced monomerization of HSPB1 peaks at 30 min after heat shock, with the protein being predominantly present as monomers at that time point (Fig. 5*B*). At 60 min after heat
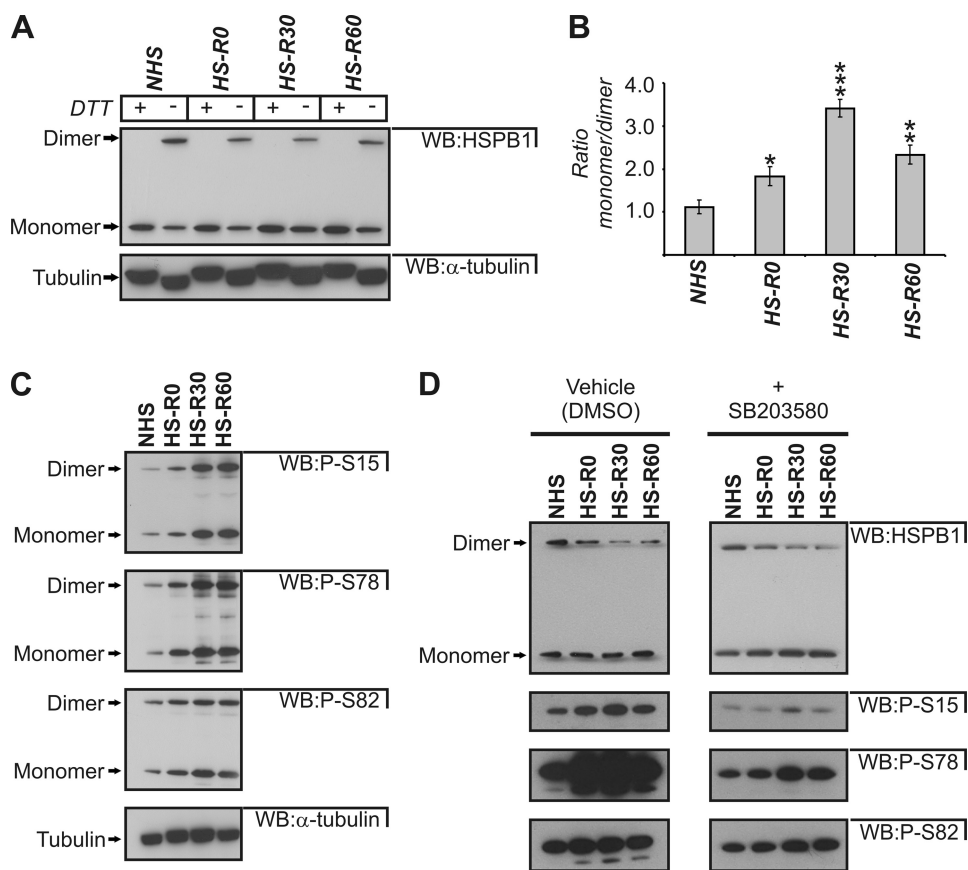
FIGURE 5. **Heat activation-induced monomerization of wild-type HSPB1.** Cells expressing wild-type HSPB1 were heat-shocked for 30 min at 44 °C and allowed to recover for different time periods. *A*, Western blot (*WB*) showing the decrease in HSPB1 dimers after heat shock. Cell extracts under reducing and non-reducing conditions were run on gel and subjected to Western blot for HSPB1. *B*, the ratio between monomeric and dimeric bands for each condition was calculated from bands from three independent experiments. The increased monomerization of HSPB1 protein peaks at 30 min after heat shock. Results are mean values with ± S.E. *error bars*. Statistical differences to the NHS condition were tested using Student's *t* test. *C*, heat shock-induced phosphorylation of HSPB1. Using phospho-specific antibodies, we checked for the phosphorylation of HSPB1 dimers and monomers at different time points. Phosphorylated forms of HSPB1 were equally present in the dimeric and monomeric bands. *D*, the heat-induced HSPB1 monomerization is unaffected by its phosphorylation status. The heat-induced HSPB1 monomerization assay was repeated in the presence of the p38 inhibitor SB203580 or the vehicle (DMSO) control. Cells were pretreated with 20 $\mu$M SB203580 or DMSO for 2 h prior to heat shock. The inhibition of HSPB1 phosphorylation does not abolish its heat-induced monomerization behavior. *Lower panels*, control Western blots with HSPB1 phospho-specific antibodies showing the inhibition of HSPB1 phosphorylation by treatment with SB203580. *, $p < 0.05$; **, $p < 0.01$; ***, $p < 0.001$; *NHS*, non-heat-shocked; *HS-R0*, heat shock and no recovery; *HS-R30*, heat shock and 30-min recovery; *HS-R60*, heat shock and 60-min recovery; *P-S15*, HSPB1 phosphoserine 15; *P-S78*, HSPB1 phosphoserine 78; *P-S82*, HSPB1 phosphoserine 82.

shock, the dimeric state starts to be restored. At 24 h after heat shock, the dimeric state is fully restored (data not shown). This result corroborates the hypothesis that the increased monomerization presented by the R127W, S135F, and R136W mutations is responsible for their hyperactivation. The same experiment was repeated for the R127W and S135F mutations. As expected, both mutants maintained the heat shock-induced monomerization pattern shown by the wild-type protein (supplemental Fig. S5).

We also investigated whether monomerization of HSPB1 is driven by phosphorylation of its known phosphorylation sites (Ser-15, Ser-78, and Ser-82). Literature data show that HSPB1 is phosphorylated by the p38/MAPKAP kinase 2/3 pathway and that its phosphorylation level reaches a plateau around 30 min after heat shock (34–36). Western blots using phospho-specific

antibodies confirmed this phosphorylation kinetics and showed that the phosphorylated forms of HSPB1 were equally present in both dimeric and monomeric forms, indicating that HSPB1 phosphorylation is not the driving force of monomerization (Fig. 5*C*). To further rule out the effect of phosphorylation, we repeated this experiment under conditions where HSPB1 is not phosphorylated (*i.e.* by using the specific p38 inhibitor SB203580). As can be seen in Fig. 5*D*, both basal and heat-induced HSPB1 phosphorylation levels were efficiently abolished by treatment with SB203580. However, inhibition of HSPB1 phosphorylation did not affect the heat-induced monomerization pattern of HSPB1 (Fig. 5*D*). Taken together, these results show that the monomerization of HSPB1 is not promoted directly by phosphorylation of any of these three serine residues.

## DISCUSSION

In 2004, our group discovered that mutations in the small heat shock protein HSPB1 are linked to CMT type 2F and distal hereditary motor neuropathy (2). Interestingly, aberrant chaperone activity had been associated before with neurodegenerative disorders (26). Disease-causing mutations in HSPs generally cause loss of their protective chaperone activity and as such lead to protein misfolding and aggregation. Among the sHSPs, lower chaperone activity has been described for the autosomal dominant cataract and desmin-related myopathy causing mutations in $\alpha$A-crystallin and $\alpha$B-crystallin (25, 27, 37). Similarly, hereditary spastic paraplegia causing mutations in HSP60 causes a reduction in the activity of this protein (38). To understand the underlying pathomechanism of disease-causing mutations in HSPB1, we investigated the influence of these mutations on the biochemical properties of this protein. In contrast to other chaperonopathies, three mutations in HSPB1 (R127W, S135F, and R136W) led to a higher, rather than a reduced, chaperone activity of the mutant protein when compared with the wild-type protein. The non-pathogenic variant S156Y and two other point mutations, T151I and P182L, did not affect HSPB1 chaperone activity. Additionally, the enhanced chaperone activity of the R127W, S135F, and R136W mutations was associated with a dimerization deficit and an enhanced binding to their client proteins.

Small heat shock proteins are present within cells in a dynamic equilibrium between oligomeric and dimeric states. Which state is the active form of these proteins or how they sense unfolded substrates is still not clear. We observed that the increased thermotolerance and *in vivo* chaperone activity of the HSPB1 mutants R127W and S135F was accompanied by a partial loss of dimerization and consequently a shift toward the monomeric state. We could couple these two phenomena by showing that activation of wild-type HSPB1 is also accompanied by an increase in the monomeric fraction of the protein. Supporting this result, it has recently been shown that the αB-crystallin mutation R120G, which causes a decrease in chaperone activity, results in increased stability of the protein dimer (21). Although the HSPB1 mutations R127W and S135F are present predominantly as monomers, they still form oligomers, showing that dimer dissociation does not necessarily result in oligomer dissociation. Actually, our SEC results revealed that the mutants R127W and S135F present a slightly higher propensity to be in the oligomeric state compared with the wild type. Therefore, we believe that the mutant HSPB1 monomers are also inserted into oligomeric structures. Corroborating with this hypothesis, Benesch *et al.* (39) recently showed that the chaperone activity of αA-crystallin and αB-crystallin is regulated by the amount of monomers within the oligomers. Oligomers formed by monomers, instead of just dimers, would be more active due to the exposition of hydrophobic surfaces previously embedded into the dimer interface. The increased exposition of hydrophobic surfaces would then result in higher substrate affinity and consequently increased chaperone function. In line with these data, we observed that mutants R127W, S135F, and R136W show an excessive binding to their client proteins, even under rest conditions. This result suggests that the regulation of these mutants is lost, which might result in unrequired formation of sHSP-substrate complexes, possibly interfering with their normal function. The mutation R136W, which presented a slightly higher chaperone activity, showed a normal SEC distribution and, interestingly, a loss of dimerization exclusively with the endogenous wild-type HSPB1 protein. Because CMT2F is an autosomal dominant disease, in patients, it is expected that the ratio between the mutant and the normal protein will be 1:1. Therefore it is possible that at equimolar conditions with the endogenous wild-type protein, the overall balance of dimers and monomers in the cells expressing the R136W mutations will be disturbed in a way similar to what is happening with the mutations R127W and S135F.

By using the recently published αB-crystallin structure (21), we were able to model the HSPB1 structure and evaluate the consequences of the CMT-causing mutations. Our analysis predicted a dimerization deficit mechanism for the R127W and S135F mutations, whereas no clear explanation was found for the behavior of the R136W mutation. Despite the high similarity between HSPB1 and αB-crystallin, the confirmation of the structural mechanisms leading to the hyperactivation of these mutations awaits resolution of the crystal structure of wild-type and mutant HSPB1.

Whether the increased chaperone activity of S135F, R127W, and R136W is actually disease-causing is unclear at this point.

Because other CMT-linked mutations behave neutrally in our chaperone assays, either the increased activity is not relevant for the disease, or it shows that different pathomechanisms for different CMT mutations are operational. The latter hypothesis is supported by the fact that patients carrying the mutations T151I and P182L were described with a predominant motor neuropathy (distal hereditary motor neuropathy) (2), whereas some patients carrying the mutations R127W, S135F, and R136W presented motor and sensory symptoms (CMT2) (2, 40, 41). The mutation P182L is a clinically more severe mutation (2, 41), and the expression of this mutation is by itself a stress to the cells. Our stable cells look smaller (data not shown), and previous studies have shown that this mutant protein forms large intracellular aggregates (42).

In conclusion, we demonstrated that in contrast to several other chaperonopathies, CMT-causing mutations in HSPB1 lead to increased chaperone activity and enhanced binding to their client proteins. Furthermore, this hyperactivity appears to be caused by an increased monomerization of HSPB1, strongly suggesting that the monomer is the active state of this protein. The link between the increased chaperone activity of HSPB1 mutants and the etiology of CMT remains to be proven. We favor the hypothesis that the increased chaperone activity is not by itself disease-causing but rather an aberrant binding with a neuron-specific partner due to the protein hyperactivity. Therefore, we are currently following up to determine if neuron-specific interaction partners of HSPB1 are targeted specifically by CMT-causing mutations. Because HSPB1 is involved in a series of normal and pathogenic biological processes, a better understanding of the biology of this protein can be of great help toward the development of therapies for a multitude of disorders.

## REFERENCES

1. Barisic, N., Claeys, K. G., Sirotković-Skerlev, M., Löfgren, A., Nelis, E., De Jonghe, P., and Timmerman, V. (2008) *Ann. Hum. Genet.* **72,** 416–441
2. Evgrafov, O. V., Mersiyanova, I., Irobi, J., Van Den Bosch, L., Dierick, I., Leung, C. L., Schagina, O., Verpoorten, N., Van Impe, K., Fedotov, V., Dadali, E., Auer-Grumbach, M., Windpassinger, C., Wagner, K., Mitrovic, Z., Hilton-Jones, D., Talbot, K., Martin, J. J., Vasserman, N., Tverskaya, S., Polyakov, A., Liem, R. K., Gettemans, J., Robberecht, W., De Jonghe, P., and Timmerman, V. (2004) *Nat. Genet.* **36,** 602–606
3. Houlden, H., Laura, M., Wavrant-De Vrièze, F., Blake, J., Wood, N., and Reilly, M. M. (2008) *Neurology* **71,** 1660–1668
4. Haslbeck, M., Franzmann, T., Weinfurtner, D., and Buchner, J. (2005) *Nat. Struct. Mol. Biol.* **12,** 842–846
5. Lelj-Garolla, B., and Mauk, A. G. (2006) *J. Biol. Chem.* **281,** 8169–8174
6. Lavoie, J. N., Lambert, H., Hickey, E., Weber, L. A., and Landry, J. (1995) *Mol. Cell. Biol.* **15,** 505–516
7. Shashidharamurthy, R., Koteiche, H. A., Dong, J., and McHaourab, H. S. (2005) *J. Biol. Chem.* **280,** 5281–5289
8. Franzmann, T. M., Wühr, M., Richter, K., Walter, S., and Buchner, J.

(2005) *J. Mol. Biol.* **350,** 1083–1093

9. Borrelli, M. J., Bernock, L. J., Landry, J., Spitz, D. R., Weber, L. A., Hickey, E., Freeman, M. L., and Corry, P. M. (2002) *Cell Stress Chaperones* **7,** 281–296

10. Charette, S. J., Lavoie, J. N., Lambert, H., and Landry, J. (2000) *Mol. Cell. Biol.* **20,** 7602–7612

11. Paul, C., Manero, F., Gonin, S., Kretz-Remy, C., Virot, S., and Arrigo, A. P. (2002) *Mol. Cell. Biol.* **22,** 816–834

12. Huot, J., Houle, F., Spitz, D. R., and Landry, J. (1996) *Cancer Res.* **56,** 273–279

13. Cuesta, R., Laroia, G., and Schneider, R. J. (2000) *Genes Dev.* **14,** 1460–1470

14. Dierick, I., Irobi, J., De Jonghe, P., and Timmerman, V. (2005) *Ann. Med.* **37,** 413–422

15. Der Perng, M., and Quinlan, R. A. (2004) *Curr. Biol.* **14,** R625–R626

16. Weckx, S., Del-Favero, J., Rademakers, R., Claes, L., Cruts, M., De Jonghe, P., Van Broeckhoven, C., and De Rijk, P. (2005) *Genome Res.* **15,** 436–442

17. Salmon, P., and Trono, D. (2006) *Current Protocols in Neuroscience*, Unit 12.10, John Wiley & Sons, Inc., New York

18. Tsai, A., and Carstens, R. P. (2006) *Nat. Protoc.* **1,** 2820–2827

19. Benjamini, Y., and Hochberg, Y. (1995) *J. R. Stat. Soc. Series B Stat. Methodol.* **57,** 289–300

20. Nollen, E. A., Brunsting, J. F., Roelofsen, H., Weber, L. A., and Kampinga, H. H. (1999) *Mol. Cell. Biol.* **19,** 2069–2079

21. Bagnéris, C., Bateman, O. A., Naylor, C. E., Cronin, N., Boelens, W. C., Keep, N. H., and Slingsby, C. (2009) *J. Mol. Biol.* **392,** 1242–1252

22. Schymkowitz, J., Borg, J., Stricher, F., Nys, R., Rousseau, F., and Serrano, L. (2005) *Nucleic Acids Res.* **33,** W382–W388

23. Arnold, K., Bordoli, L., Kopp, J., and Schwede, T. (2006) *Bioinformatics* **22,** 195–201

24. Collins, T. J. (2007) *BioTechniques* **43,** Suppl. 1, 25–30

25. Bova, M. P., Yaron, O., Huang, Q., Ding, L., Haley, D. A., Stewart, P. L., and Horwitz, J. (1999) *Proc. Natl. Acad. Sci. U.S.A.* **96,** 6137–6142

26. Muchowski, P. J., and Wacker, J. L. (2005) *Nat. Rev. Neurosci.* **6,** 11–22

27. Andley, U. P., Patel, H. C., and Xi, J. H. (2002) *J. Biol. Chem.* **277,** 10178–10186

28. Mchaourab, H. S., Berengian, A. R., and Koteiche, H. A. (1997) *Biochemistry* **36,** 14627–14634

29. Berengian, A. R., Parfenova, M., and Mchaourab, H. S. (1999) *J. Biol. Chem.* **274,** 6305–6314

30. van Montfort, R. L., Basha, E., Friedrich, K. L., Slingsby, C., and Vierling, E. (2001) *Nat. Struct. Biol.* **8,** 1025–1030

31. Kim, K. K., Kim, R., and Kim, S. H. (1998) *Nature* **394,** 595–599

32. Stamler, R., Kappé, G., Boelens, W., and Slingsby, C. (2005) *J. Mol. Biol.* **353,** 68–79

33. Hilario, E., Teixeira, E. C., Pedroso, G. A., Bertolini, M. C., and Medrano, F. J. (2006) *Acta Crystallogr. Sect. F Struct. Biol. Cryst. Commun.* **62,** 446–448

34. Chrétien, P., and Landry, J. (1988) *J. Cell. Physiol.* **137,** 157–166

35. Landry, J., Lambert, H., Zhou, M., Lavoie, J. N., Hickey, E., Weber, L. A., and Anderson, C. W. (1992) *J. Biol. Chem.* **267,** 794–803

36. Guay, J., Lambert, H., Gingras-Breton, G., Lavoie, J. N., Huot, J., and Landry, J. (1997) *J. Cell Sci.* **110,** 357–368

37. Cobb, B. A., and Petrash, J. M. (2000) *Biochemistry* **39,** 15791–15798

38. Bross, P., Naundrup, S., Hansen, J., Nielsen, M. N., Christensen, J. H., Kruhøffer, M., Palmfeldt, J., Corydon, T. J., Gregersen, N., Ang, D., Georgopoulos, C., and Nielsen, K. L. (2008) *J. Biol. Chem.* **283,** 15694–15700

39. Benesch, J. L., Ayoub, M., Robinson, C. V., and Aquilina, J. A. (2008) *J. Biol. Chem.* **283,** 28513–28517

40. Tang, B., Liu, X., Zhao, G., Luo, W., Xia, K., Pan, Q., Cai, F., Hu, Z., Zhang, C., Chen, B., Zhang, F., Shen, L., Zhang, R., and Jiang, H. (2005) *Arch. Neurol.* **62,** 1201–1207

41. Dierick, I., Baets, J., Irobi, J., Jacobs, A., De Vriendt, E., Deconinck, T., Merlini, L., Van den Bergh, P., Rasic, V. M., Robberecht, W., Fischer, D., Morales, R. J., Mitrovic, Z., Seeman, P., Mazanec, R., Kochanski, A., Jordanova, A., Auer-Grumbach, M., Helderman-van den Enden, A. T., Wokke, J. H., Nelis, E., De Jonghe, P., and Timmerman, V. (2008) *Brain* **131,** 1217–1227

42. Ackerley, S., James, P. A., Kalli, A., French, S., Davies, K. E., and Talbot, K. (2006) *Hum. Mol. Genet.* **15,** 347–354